Journal of Magnetic Resonance 201 (2009) 157–164

Contents lists available at ScienceDirect

Journal of Magnetic Resonance

journal homepage: www.elsevier.com/locate/jmr

^{1}H–^{19}F spin–lattice relaxation spectroscopy: Proton tunnelling in the hydrogen bond studied by field-cycling NMR

D.L. Noble [a], A. Aibout [b], A.J. Horsewill [a,*]

[a] School of Physics & Astronomy, University of Nottingham, University Park, Nottingham, England NG7 2RD, UK
[b] Laboratoire de Spectroscopie des Materiaux, Université de Mostaganem B.P. 227, Mostaganem 27000, Algeria

ARTICLE INFO

Article history:
Received 14 May 2009
Revised 24 August 2009
Available online 6 September 2009

Keywords:
Field-cycling NMR
Spin–lattice relaxation
Cross-relaxation
Proton tunnelling
Molecular dynamics
Heteronuclear interactions

ABSTRACT

Proton tunnelling in the hydrogen bonds of two fluorine substituted benzoic acid dimers has been investigated using field-cycling NMR relaxometry. The close proximity of the ^{19}F nuclei to the hydrogen bond protons introduces heteronuclear ^{19}F–^{1}H dipolar interactions into the spin–lattice relaxation processes. This renders the ^{1}H magnetisation–recovery biexponential and introduces multiple spectral density components into the relaxation matrix characterised by frequencies that are sums and differences of the ^{19}F and ^{1}H Larmor frequencies. Using field-cycling NMR pulse sequences that measure the spin–lattice relaxation and cross-relaxation rates we demonstrate how some of these multiple spectral density components can be separately resolved. This leads to an accurate determination of the correlation times that characterise the proton tunnelling motion. A broad spectrum of relaxation behaviour is illustrated and explored in the chosen samples and the investigation is used to explore the theory and practise of field-cycling NMR relaxometry in cases where heteronuclear interactions are significant.

1. Introduction

Proton transfer is important to many chemical and biological processes including those important to maintaining life. It is also one of the simplest chemical reactions and since it involves the displacement of an atom with low mass the system is significant to understanding the role of quantum tunnelling in chemical and biological kinetics. For example, in the area of enzyme catalysis, isotopic substitution of the hydrogen provides insight into the influence such quantum effects may have on the kinetics at ambient temperature [1,2].

For fundamental investigations of the proton transfer process, solid-state NMR is well-suited to characterising the hydrogen dynamics [3–7]. The role of tunnelling can be a complex one so it is important to investigate model systems to gain fundamental insight into the proton transfer process as well as to provide a platform for a deeper exploration of the experimental protocols used to investigate the dynamics. One such model system is the concerted double proton transfer in the hydrogen bonds of carboxylic acid dimers in the solid state [8–13], Fig. 1, where incoherent tunnelling is shown to dominate at low temperature. Here, NMR relaxometry has been particularly effective in characterising the dynamics and when the frequency and magnetic field domain is exploited through magnetic field-cycling, spin–lattice relaxation time measurements can provide highly accurate measurements of molecular correlation times and deep insight into the mechanisms of molecular motion [7,14,15].

For homonuclear spin systems, the magnetic field dependence of the spin–lattice relaxation rate, $T_1^{-1}(B)$, maps out the spectral density directly, comprising two components, one which samples the spectral density at the Larmor frequency, ω_L, and the second which samples at $2\omega_L$ [8,16]. For proton transfer in the hydrogen bond, the spectral density is shown to have Lorentzian form demonstrating that the tunnelling motion of the hydrogen between the two potential wells that characterise the hydrogen bond is a stochastic process [11]. Accordingly, the correlation time for proton transfer can be determined with an accuracy better than 5% from the half-width of the $T_1^{-1}(B)$ profile. This has provided great insight into our understanding of proton tunnelling in the hydrogen bond and the smooth evolution from the regime of pure tunnelling at low temperature to one of pseudo-classical barrier hopping at high temperature [9,10,12,13,17–20].

When the samples contain additional magnetic nuclei and can no longer be characterised as homonuclear, further spin–lattice relaxation pathways are introduced. These arise from the modulation of heteronuclear interactions between the multiple spins systems as the hydrogen atoms undergo their proton transfer motion. The spin–lattice relaxation therefore acquires additional components which sample the spectral density at sums and differences of the Larmor frequencies of the spin systems [21]. This introduces new challenges into the quantitative interpretation of spin–lattice

* Corresponding author. Fax: +44 (0) 115 951 5180.
E-mail address: a.horsewill@nottingham.ac.uk (A.J. Horsewill).

1090-7807/$ - see front matter © 2009 Elsevier Inc. All rights reserved.
doi:10.1016/j.jmr.2009.09.001

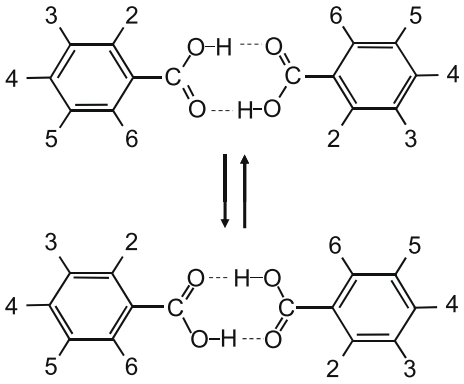

Fig. 1. Double proton transfer interchanging the two tautomers that characterise the fluoro-substituted benzoic acid dimers. Powder samples of 2,6-difluorobenzoic acid and 2,3,5,6-tetrafluorobenzoic acid were investigated; the ^{19}F substitution sites are labelled on the phenyl ring.

relaxation data and the determination of the proton transfer rates. In a recent paper we showed how field-cycling measurements of the cross-relaxation process linking two Zeeman systems can be used to extract accurate correlation times [22]. In this present paper we undertake a wider exploration of heteronuclear ^{19}F–^{1}H spin–lattice relaxation including both diagonal and cross-relaxation components, showing how the multiple spectral density components can be resolved from the field-dependence data.

The study has been undertaken on two fluorine substituted derivatives of benzoic acid dimers which exhibit concerted double proton transfer ($C_6H_{5-x}F_xCOOH$: x = 2,4). The proton transfer process mediates the interchange between the two tautomer configurations of the dimer, Fig. 1. The fluorine atoms are substituted on the phenyl ring so with ^{19}F nuclei in close proximity to the dynamical ^{1}H nuclei, the investigated materials enable an exploration of a range of spin–lattice relaxation behaviour arising from heteronuclear interactions and the experimental protocols required to extract accurate data on the ^{1}H dynamics. This provides an additional motivation for this investigation; to explore and optimise the efficacy of field-cycling NMR relaxometry in cases where heteronuclear interactions are significant.

2. Theory

2.1. Spin–lattice relaxation

The spin–lattice relaxation equations appropriate to proton transfer in the hydrogen bond have been described in the literature. These have been reviewed in [7] so we shall only summarise the main results here. Consider two nuclear spin systems, labelled I and S, both with spin ½. In this paper the ^{1}H spins will be assigned to spins I and the ^{19}F nuclei to spins S. If the equilibrium polarisations are designated as I_0 and S_0 then the time evolution of the spin polarisations, $\langle I_z\rangle$, $\langle S_z\rangle$ is governed by spin–lattice relaxation within this manifold of interacting spins as follows [21],

$$\begin{bmatrix} \frac{d}{dt}\langle I_z\rangle \\ \frac{d}{dt}\langle S_z\rangle \end{bmatrix} = -\begin{pmatrix} \rho_I & \sigma \\ \sigma & \rho_S \end{pmatrix}\begin{bmatrix} (\langle I_z\rangle - I_0) \\ (\langle S_z\rangle - S_0) \end{bmatrix} \tag{1}$$

Cross-relaxation between the Zeeman reservoirs of I and S has relaxation rate σ while the diagonal elements ρ_I and ρ_S define the spin–lattice relaxation rates of each Zeeman reservoir. Efficient spin diffusion within each reservoir is implicitly assumed in Eq. (1).

The relaxation is dominated by the modulation of the homonuclear and heteronuclear dipolar interactions and the elements of the relaxation matrix $\boldsymbol{R} = \begin{pmatrix} \rho_I & \sigma \\ \sigma & \rho_S \end{pmatrix}$ are defined by correlation functions and spectral density functions given elsewhere [8,21]. Evaluating these for double proton transfer in the hydrogen bond we obtain for powder samples [7,13,23,24],

$$\begin{aligned}\rho_I = {} & C_{FH}\tfrac{4a}{(1+a)^2}(L(\omega_H-\omega_F,\tau_c)+3L(\omega_H,\tau_c)+6L(\omega_H+\omega_F,\tau_c)) \\ & + C_{HH}\tfrac{4a}{(1+a)^2}(L(\omega_H,\tau_c)+4L(2\omega_H,\tau_c))\end{aligned} \tag{2}$$

$$\sigma = C_{FH}\frac{4a}{(1+a)^2}(-L(\omega_H-\omega_F,\tau_c)+6L(\omega_H+\omega_F,\tau_c)) \tag{3}$$

$$\rho_S = C_{FH}\frac{4a}{(1+a)^2}(L(\omega_F-\omega_H,\tau_c)+3L(\omega_F,\tau_c)+6L(\omega_F+\omega_H,\tau_c)) \tag{4}$$

where $a = \exp(A/k_BT)$ and A is the energy asymmetry (Gibbs free energy) of the double well potential that characterises the proton transfer in the hydrogen bonds. The Lorentzian relaxation lineshapes, $L(\omega,\tau_c) = \tau_c/(1+\omega^2\tau_c^2)$ arise from the stochastic nature of the barrier crossing process in both quantum tunnelling (low-temperature) and pseudo-classical (high-temperature) regimes [9,11]. C_{FH} and C_{HH} are dipolar constants determined by lattice sums of heteronuclear ^{1}H–^{19}F and homonuclear ^{1}H interactions, respectively. Since the dipole–dipole interactions dominate, the spin–lattice relaxation is dependent on the orientation of the B-field with respect to the unit cell axes. The expressions for single crystal samples have been given in [13], however, it is well established that an average over all possible orientations of the B-field [7,8] describes well the spin–lattice relaxation time for a powder sample; explicit powder average expressions for the dipolar constants in terms of the molecular geometry and the dipolar contact distances have been given in [23].

As will become apparent, a significant feature of ^{1}H–^{19}F systems is the similarity of the respective magnetogyric ratios γ_H and γ_F which means the Larmor frequencies of the two spin systems differ by only 5.9%.

In general, the coupled differential Eq. (1) have bi-exponential solutions,

$$\begin{aligned}\langle I_z\rangle &= I_0(c_1^I\exp(-R_1t)+c_2^I\exp(-R_2t))+I_0 \\ \langle S_z\rangle &= S_0(c_1^S\exp(-R_1t)+c_2^S\exp(-R_2t))+S_0\end{aligned} \tag{5}$$

with time-evolution defined by the relaxation rates R_1 and R_2 which are eigenvalues of $\boldsymbol{R}$,

$$R_{1,2} = \frac{1}{2}((\rho_I+\rho_S)\pm\sqrt{(\rho_I-\rho_S)^2+4\sigma^2}) \tag{6}$$

The weighting coefficients $c_{1,2}^{I,S}$ depend on the polarisation states at time $t = 0$ [24,25]. Although in Eq. (1) it is the spin polarisations that equilibrate, experimentally measurements are made of the nuclear magnetisations which are proportional to the polarisations.

2.2. Double proton transfer

Adapting the theory of Skinner and Trommsdorff [17] we may write the temperature dependence of the inverse correlation time for double proton transfer as [11,26],

$$\tau_c^{-1} = k_0\coth\left(\frac{A}{2k_BT}\right)+\tau_{exc}^{-1}\exp\left(\frac{-\Delta E_{exc}}{k_BT}\right)+\tau_0^{-1}\exp\left(\frac{-\Delta E_{act}}{k_BT}\right) \tag{7}$$

Here, the first term on the right hand side describes phonon assisted tunnelling in the ground state with tunnelling rate k_0. The third term is an Arrhenius law describing pseudo-classical barrier hopping with activation energy ΔE_{act} and attempt frequency τ_0^{-1}. The second term defines the contribution made to the proton

transfer rate by through barrier tunnelling via an excited state that has energy approximately ΔE_{exc} above the ground state; this pathway has an effective tunnelling rate τ_{exc}^{-1}. The model is discussed in more detail in Refs. [11,12,17,19,26].

3. Experimental details

Two fluorine substituted carboxylic acid samples were obtained from Aldrich and their spin–lattice relaxation properties investigated in the powdered state. The molecular structures of 2,6-difluorobenzoic acid ($C_6H_3F_2COOH$) and 2,3,5,6-tetrafluorobenzoic acid (C_6HF_4COOH) are illustrated in Fig. 1 along with the labelling scheme for fluorine substitution on the phenyl ring. These benzoic acid derivatives form dimers connected by a pair of bridging hydrogen bonds. The two particular samples were chosen to exhibit a range of relaxation behaviour which we shall later refer to as 'diagonal' and 'cross-relaxation', thereby facilitating a full exploration of field-cycling NMR relaxometry in the context of heteronuclear interactions.

The ^{1}H spin–lattice relaxation was investigated as a function of magnetic field and temperature using the Nottingham field-cycling NMR spectrometer and experimental procedures described in the literature [7,27]. Two field-cycling NMR pulse sequences were employed, illustrated in Fig. 2. One is a field-cycling adaptation of a saturation–recovery sequence, Fig. 2a. This was used to record the magnetisation–recovery curves from which the relaxation rates R_1 and R_2 were extracted by fitting to Eq. (5). In order that a systematic sequence of data is obtained, when making measurements of ^{1}H magnetisation–recovery it is essential for the initial state of the ^{19}F Zeeman reservoir to be the same at the beginning of each recovery period. This can be achieved by either saturating the ^{19}F spins or by preparing the ^{19}F polarisation to be at equilibrium. In field-cycling sequences it was usually more time efficient to saturate the ^{19}F spins as in Fig. 2a. The resonant frequency of the NMR spectrometer was 36.35 MHz so that measurements of the ^{1}H magnetisation were recorded at the field $B = 0.853T$.

^{1}H–^{19}F cross–relaxation was measured using the sequence shown in Fig. 2b. The procedures are discussed in Ref. [22]; following polarisation of the ^{1}H spins, the ^{19}F spins are saturated and the subsequent evolution of the ^{1}H spins is monitored as a function of time as energy flows between the two Zeeman reservoirs. The polarisation period, τ_{pol}, and polarisation field, B_{pol}, are chosen so that the initial ^{1}H polarisation is equal to its equilibrium polarisation at the recovery field B_r.

The measurements were conducted in the solid state where dipole–dipole interactions dominate the NMR lineshape. Therefore, a single broad line with half-width of order 25 kHz is observed in the ^{1}H NMR spectrum; this masks any differences in chemical shift that characterise the different protons. Due to the strong dipolar coupling, spin diffusion is efficient within the ^{1}H and ^{19}F Zeeman systems so that each nuclear species is characterised by a single temperature.

For all spin–lattice relaxation sequences the magnetisation–recovery curves were sampled using equal steps in the logarithm of recovery time, τ_r. To accurately extract two relaxation rates from fits to bi-exponential data it was necessary to record 30–40 data points for each curve.

4. Experimental results

For the purposes of presenting the results we shall classify the behaviour according to whether cross relaxation is significant or not. If significant, then the polarisation–recovery is observed to be bi-exponential and disturbing the spin state of one group of spins, for example by r.f. irradiation of ^{19}F, leads to a measurable perturbation of the polarisation state of the second spin system, in this case ^{1}H. If there is no significant cross-relaxation then the relaxation is dominated by the diagonal terms in Eq. (1) and a single exponential function fits well to the observed polarisation–recovery.

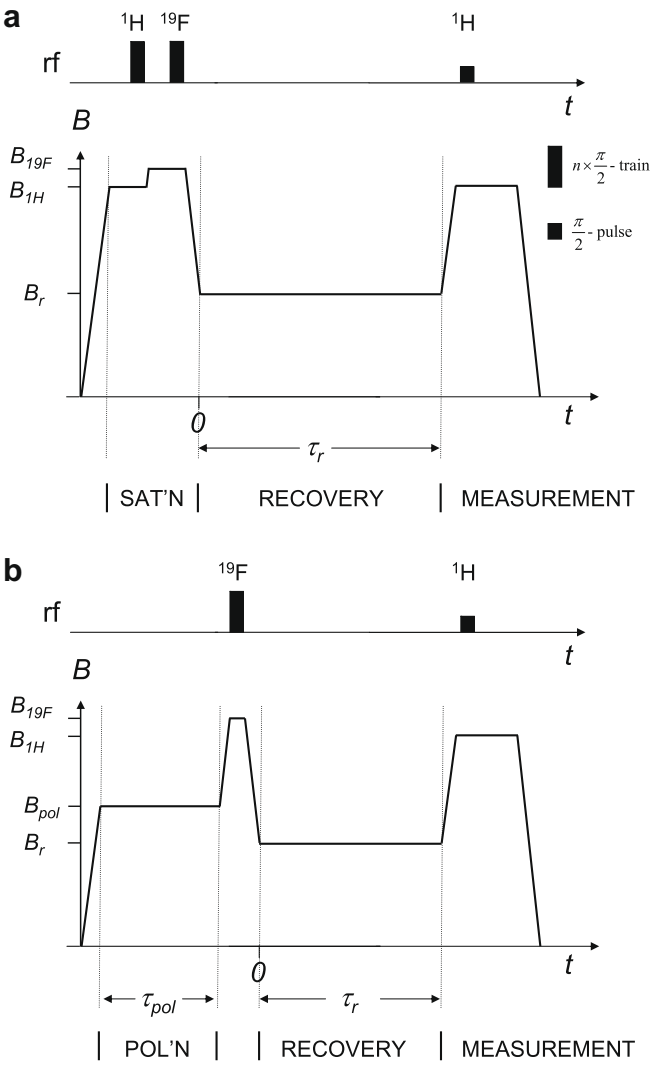

Fig. 2. Field-cycling NMR pulse sequences for measurement of spin–lattice relaxation in heteronuclear systems: (a) a saturation–recovery pulse sequence where the initial state of the system is prepared as $\langle I_z\rangle_{t=0} = 0$, $\langle S_z\rangle_{t=0} = 0$; (b) a cross-relaxation pulse sequence where the initial state of the system is prepared as $\langle I_z\rangle_{t=0} = I_0^{(B_r)}$, $\langle S_z\rangle_{t=0} = 0$. Measurements of the ^{1}H magnetisation are made using a $\pi/2$ -pulse.

4.1. Diagonal relaxation behaviour

4.1.1. 2,6-Difluorobenzoic acid (2,6-DFBA)

At all temperatures the ^{1}H magnetisation–recovery curves were observed to be single exponential functions within experimental uncertainties. The temperature dependence of the ^{1}H spin–lattice relaxation rate, T_1^{-1}, recorded at $B_r = 0.853T$ is plotted as a function of inverse temperature in Fig. 3. In this fixed field mode where no field-cycling was involved, the ^{19}F spins were prepared at equilibrium. The curve has a shape characteristic of many carboxylic acid dimers. There is a maximum in T_1^{-1} at approximately 90 K and the curve has a smaller gradient on the low temperature side of the relaxation rate maximum compared with that at high temperature. As with similar systems, the slope on the high temperature side is

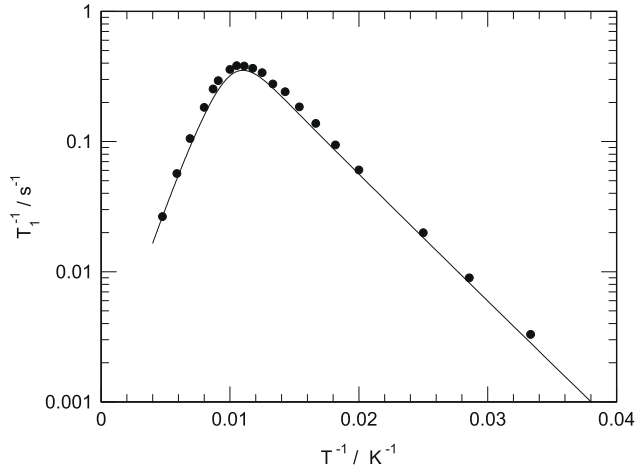

Fig. 3. The ^{1}H spin–lattice relaxation rate T_1^{-1} in 2,6-DFBA as a function of inverse temperature. The solid line is the fit assuming the correlation rate has the analytical form given in Eq. (7) where tunnelling dominates at low temperature; see text for details.

determined by the Arrhenius law governing pseudo-classical barrier hopping whereas at low temperature the correlation time is temperature independent and the slope is determined by the Boltzmann factor, $4a/(1+a)^2$, (Eq. (2)) arising from the energy asymmetry of the double well potential.

The magnetic field dependence of the ^{1}H spin–lattice relaxation rate has been plotted in Fig. 4 for 8 temperatures in the range $30 \leqslant T \leqslant 115$K. The data have been reflected in the $B = 0$ axis to accentuate the Lorentzian character of the spectral density components. Since the magnetisation–recovery curves are single exponential we can infer that the off-diagonal elements of the relaxation matrix are small compared with the diagonal elements. The corollary is that the homonuclear spectral density terms dominate over the heteronuclear ones, $C_{HH} > C_{FH}$. To examine the validity of this approximation the function

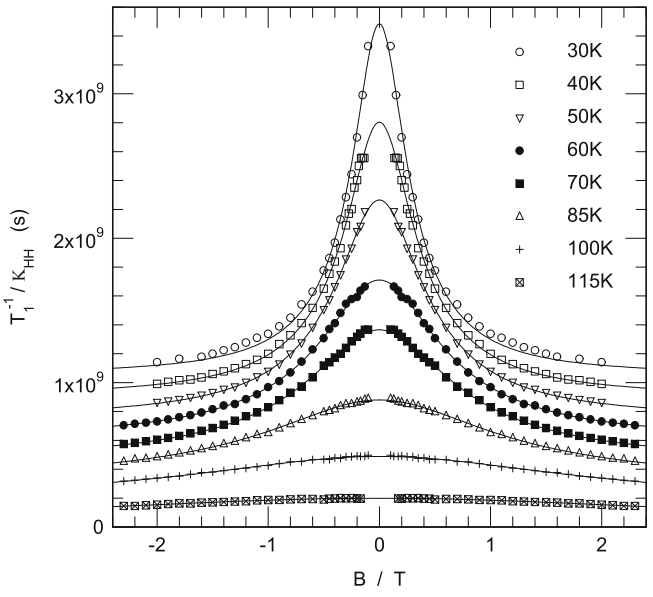

Fig. 4. The magnetic field dependence of the ^{1}H spin–lattice relaxation rate measured in 2,6-DFBA at a variety of temperatures. The normalised function T_1^{-1}/K_{HH} is plotted. The curves for each temperature are successively offset by 1.5×10^8s. The solid lines are the fits with Eq. (8) assuming the homonuclear spectral density functions dominate. The inverse correlation times, τ_c^{-1}, for proton transfer are determined from the widths of the Lorentzian lineshapes.

$$T_1^{-1} = K_{HH}(L(\omega_H, \tau_c) + 4L(2\omega_H, \tau_c)) \tag{8}$$

which is the homonuclear part of ρ_I in Eq. (2), has been fitted to the data in Fig. 4. The amplitude

$$K_{HH} = C_{HH}\frac{4a}{(1+a)^2} \tag{9}$$

incorporates the dipolar constant and the Boltzmann factor. These provide a direct plot of the spectral density functions, Eq. (2). For presentational purposes and to normalise the effects of temperature on the spectral density amplitude, the function T_1^{-1}/K_{HH} has been plotted in Fig. 4. Fits to the data with Eq. (8) are shown in Fig. 4 with solid lines and represent the data very well. In Fig. 5 the temperature dependence of the fitted values of K_{HH} are plotted together with the best fit using Eq. (9); the best fit parameters are $C_{HH} = (2.2 \pm 0.2) \times 10^8 s^{-2}$, $A/k_B = 224 \pm 4K$. The latter is the free enthalpy and any entropy contributions are not significant within experimental error ($\approx$0.05 J mol^{-1} K^{-1}).

The best fit values of the inverse correlation time, τ_c^{-1}, are plotted in Fig. 6 (closed symbols); these data display the behaviour characteristic of tunnelling, namely the tendency for τ_c^{-1} to become temperature independent in the limit of low temperature.

4.2. Cross-relaxation behaviour

4.2.1. 2,3,5,6-Tetrafluorobenzoic acid (2,3,5,6-TFBA)

The inverse temperature dependence of the ^{1}H spin–lattice relaxation is presented in Fig. 7. The data were recorded at constant magnetic field $B_r = 0.853$ T ($\omega_H = 36.35$ MHz) using a saturation–recovery pulse sequence. The ^{1}H polarisation–recovery was bi-exponential for temperatures below approximately 100 K and the spin–lattice relaxation rates, R_1, R_2, are plotted. The ratio of the two rates was typically a factor of order ten for temperatures below 30 K. The bi-exponential behaviour is attributed to the presence of cross-relaxation pathways linking the ^{19}F and ^{1}H Zeeman systems.

The data exhibit a relaxation rate maximum at approximately 100 K with a secondary shoulder at approximately 35 K. Considering the spectral density functions Eqs. (2)–(4), the high temperature maximum can be attributed to a peak in relaxivity where $\omega_H\tau_c \approx 1$ whereas the shoulder corresponds to a correlation time where $(\omega_H - \omega_F)\tau_c \approx 1$. The latter is significantly offset in temper-

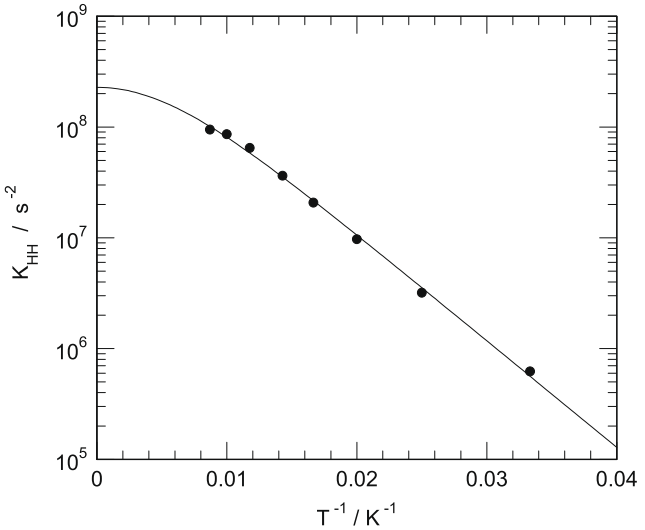

Fig. 5. The inverse temperature dependence of the amplitude of the spectral density in 2,6-DFBA, Eq. (9) determined from fits to the data in Fig. 4. The solid line is the fit from which the energy asymmetry is determined, $A/k_B = 224 \pm 4$K.

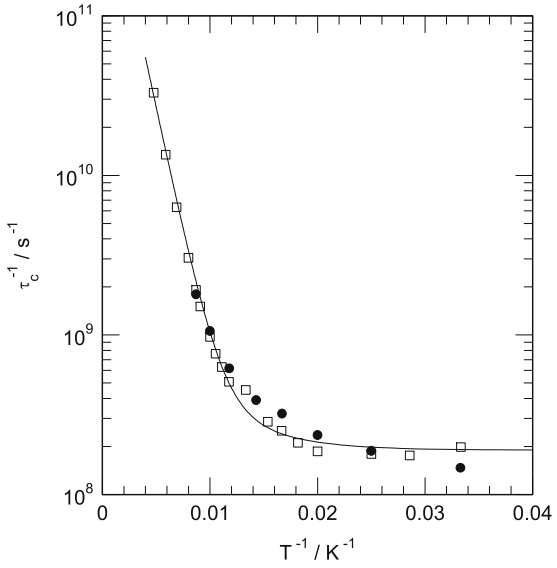

Fig. 6. The inverse correlation time τ_c^{-1} in 2,6-DFBA as a function of inverse temperature. Closed data points; determined from the fits to the spectral density data in Fig. 4. Open data points determined from inversion of Eq. (8) using the data in Fig. 3. Solid line; fit with Eq. (7).

ature from the former because the ^{1}H and ^{19}F Larmor frequencies are so similar, rendering the difference frequency $(\omega_H - \omega_F)$ much smaller than ω_H.

As for samples exhibiting diagonal relaxation behaviour, the low temperature gradient of the $\log(R_1, R_2)$ vs. $1/T$ plot provides a preliminary estimate of the energy asymmetry; the best fit value is found to be $A/k_B = 80 \pm 3$K.

Further insight into the proton transfer dynamics and the relaxation behaviour was sought by recording the magnetic field dependence through field-cycling. In reference [22] we have shown how the correlation time for proton transfer may be measured directly from the magnetic field dependence of the cross relaxation rate, σ. The latter was measured in 2,3,5,6-TFBA at a variety of magnetic field values using the cross-relaxation pulse sequence Fig 2b where the initial polarisation states of the two spin species are $\langle I_z\rangle_{t=0} = I_0^{(B_r)}$, $\langle S_z\rangle_{t=0} = 0$. In Fig. 8 a comparison is made between the ^{1}H magnetisation–recovery curves recorded using the cross-relaxation pulse sequence and the saturation–recovery pulse sequence; the data were recorded at $B = 0.75T$ and $T = 18K$. For the cross-relaxation experiment, the ^{19}F spins are saturated at time $t = 0$ and the ^{1}H spins, which begin with equilibrium populations, relax with rate R_2 as they respond to the change in the ^{19}F polarisation. This leads to a decline of approximately 40% in the ^{1}H polarisation before the ^{1}H spins begin to relax back towards equilibrium with rate R_1. In the cross-relaxation sequence the recovery of $\langle I_z\rangle$ is governed by Eq. (5) with coefficients [22]

$$c_1^I = \left(\frac{\sigma}{R_2 - R_1}\right)\frac{\gamma_F}{\gamma_H}; \quad c_2^I = -c_1^I \tag{10}$$

The magnetisation–recovery observed with the saturation–recovery pulse sequence at the same temperature and field is also characterised by Eq. (5) with the same two relaxation times, $R_1^{-1} = 247 \pm 3s$ and $R_2^{-1} = 19.1 \pm 0.8s$ but different coefficients c_i^I which in this case have the same sign.

Using the procedures described in [22] the magnetic field dependence of the off-diagonal element of the relaxation matrix, $\sigma(B)$, was determined from experiments using the cross-relaxation pulse sequence at $T = 18K$. The results are presented in Fig. 9. According to Eq. (3), the magnetic field-dependence of σ is determined by the spectral density components $L(\omega_H - \omega_F)$ and $L(\omega_H + \omega_F)$ which contribute with amplitude ratios -1 and 6, respectively. Therefore, the function determining $\sigma(B)$ is well-defined and by fitting Eq. (3) to the data in Fig. 9, the inverse correlation time has been determined;

$$\tau_c^{-1}(18K) = (9.8 \pm 0.1) \times 10^6 s^{-1}$$

In Fig. 9 the best-fit is shown with a solid line. $\sigma(B)$ exhibits a minimum at the field $B_r \simeq 0.2T$ and in the measured range the behaviour is dominated by the spectral density component $L(\omega_H - \omega_F)$, meaning $\sigma(B)$ is negative, Eq. (3). This situation arises for the ^{1}H–^{19}F system because the Larmor frequencies of the two nuclei differ by only 5.9% so that $L(\omega_H - \omega_F)$, when plotted as a function of magnetic field, appears as a broad negative component while $L(\omega_H + \omega_F)$ contributes to $\sigma(B)$ as a very much narrower, positive component [22,23].The magnetic field dependence of the spin–lattice relaxation rates R_1 and R_2 at 18 K were also recorded using the saturation–recovery pulse sequence; these were measured in

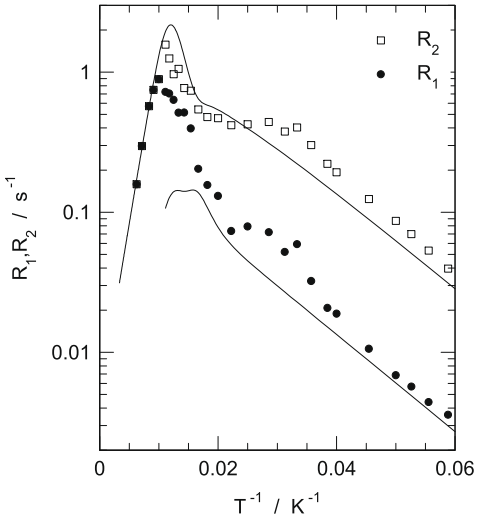

Fig. 7. The bi-exponential spin–lattice relaxation rates R_1 and R_2 in 2,3,5,6-TFBA recorded as a function of inverse temperature. The solid lines are the fit assuming the correlation rate has the analytical form given in Eq. (7) where tunnelling dominates at low temperature; see text for details.

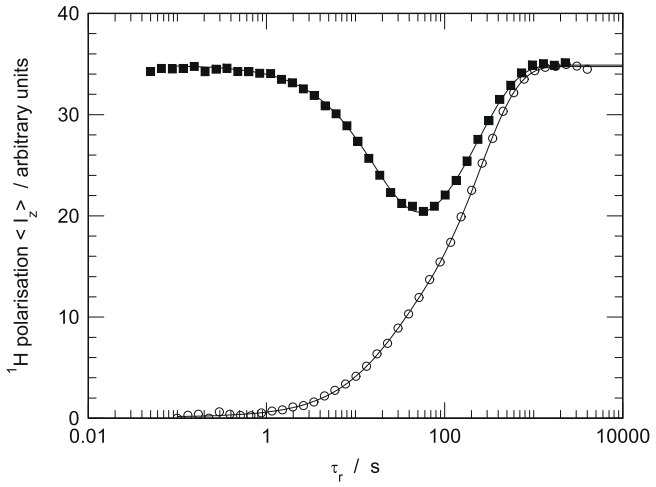

Fig. 8. ^{1}H magnetisation–recovery curves in 2,3,5,6-TFBA recorded at $B_r = 0.75T$, $T = 18$K. Closed squares: using cross-relaxation pulse sequence Fig. 2b. Open circles: using the saturation–recovery pulse sequence Fig. 2a. Solid lines: fits with the bi-exponential function Eq. (5).

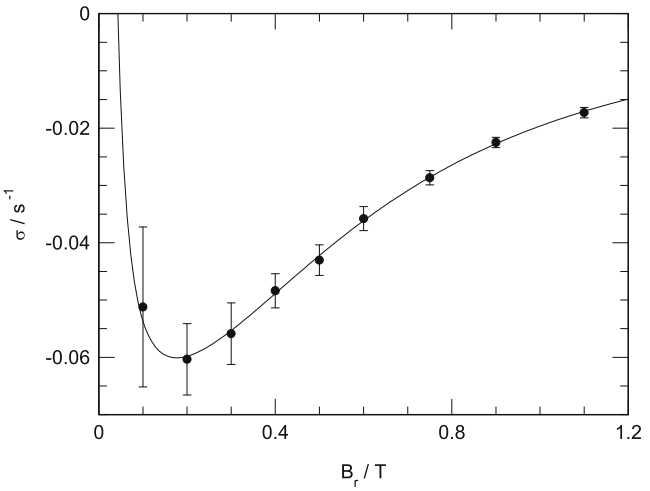

Fig. 9. The magnetic field dependence of the cross-relaxation rate σ measured at $T = 18$K in 2,3,5,6-TFBA. The solid line is the fit with the spectral density functions defined in Eq. (3) leading to $\tau_c^{-1}(18\text{K}) = (9.8 \pm 0.1) \times 10^6 \text{s}^{-1}$. In the field region studied the behaviour is dominated by the spectral density component $L(\omega_H - \omega_F, \tau_c)$ which is negative and appears very much broader than the positive component $L(\omega_H + \omega_F, \tau_c)$ that dominates at very low field.

the magnetic field range $0.02 \leqslant B_r \leqslant 1.4T$ and are presented in Fig. 10. As roots of a quadratic equation involving the various spectral density functions, Eq. (6), the field dependence of the rates R_1 and R_2 is relatively complex and cannot easily be written as an analytical function, particularly as the dipolar constants C_{FH} and C_{HH} are not known *a priori*. We shall return to an analysis of Fig. 10 in the discussion.

5. Discussion

5.1. 2,6-Difluorobenzoic acid

Given the ^{1}H spin–lattice relaxation time agrees well with Eq. (8) and accurate values of C_{HH} and A have been determined, values of τ_c^{-1} as a function of temperature have been determined from the fixed field T_1^{-1} data in Fig. 3 by inversion using Eq. (8). These have been plotted with open symbols in Fig. 6. In the overlap region, good agreement is obtained with the values measured from the magnetic field dependent, spectral density plots.

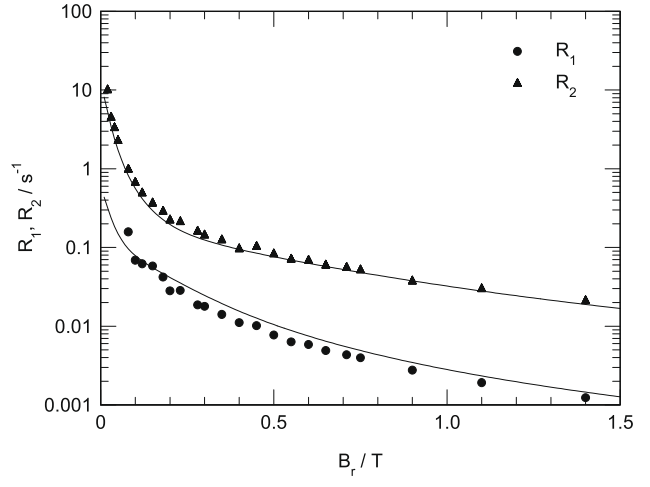

Fig. 10. The magnetic field dependence of the bi-exponential spin–lattice relaxation rates R_1 and R_2 in 2,3,5,6-TFBA recorded at $T = 18$K. The solid lines are simultaneous fits to R_1 and R_2 using Eqs. (2), (3), (4), and (6) leading to $\tau_c^{-1}(18\text{K}) = (9.8 \pm 0.1) \times 10^6 \text{s}^{-1}$. The broader spectral density component arises from $L(\omega_H - \omega_F, \tau_c)$ while the narrower component derives from the other spectral density terms defined in Eqs. (2)–(4).

The temperature dependence of the correlation rate τ_c^{-1} exhibits the characteristic features of double proton transfer in carboxylic acid dimers: at low temperature τ_c^{-1} is independent of temperature, indicating the motion is dominated by phonon assisted tunnelling in the ground state; at elevated temperatures additional through barrier tunnelling pathways become available as higher states become populated and in a high temperature limit the behaviour can be written as an Arrhenius law. At all temperatures the motion is stochastic mediated by various barrier penetration pathways. At the highest observed temperatures where the behaviour is Arrhenius the proton transfer motion may be described as 'pseudo-classical' [7]; this is characterised by an apparent activation energy that is determined by a Boltzmann average of populated well-states. However, it is known that the barrier height is much larger than this so that a formal description of classical motion characterised by over-barrier hopping is not significant even at ambient temperature (300 K) [7,12,17,19,28]. Using Eq. (7) the best fit to the data in Fig. 6 is determined as follows,

$$\tau_c^{-1}(1/T) = 1.9 \times 10^8 \coth(224/2k_BT) + 1 \times 10^9 \times \exp(-200/k_BT) + 1 \times 10^{12} \exp(-730/k_BT) \qquad (11)$$

Substituting Eq. (11) in Eq. (8) with $C_{HH} = (2.2 \pm 0.2) \times 10^8 s^{-2}$ and $A/k_B = 224 \pm 4K$ the modelled temperature dependence of the spin–lattice relaxation rate $T_1^{-1}(1/T)$ is obtained and is shown with a solid line in Fig. 3. The modelled behaviour of $T_1^{-1}(1/T)$ and $\tau_c^{-1}(1/T)$ gives good agreement with experimental data; the $T_1^{-1}(1/T)$ simulation is good to within approx 5%, corresponding to the uncertainty in the dipolar constant C_{HH}. The approximation implied in the use of Eq. (8), namely $C_{HH} > C_{FH}$, appears to be justified.

5.2. 2,3,5,6-Tetrafluorobenzoic acid

The cross-relaxation experiment provides a very effective technique for accurately measuring the inverse correlation time for proton transfer. However, as was noted earlier, by contrast with 2,6-DFBA which exhibits diagonal relaxation behaviour, to extract τ_c^{-1} from the plot of R_1 and R_2, Fig. 10, is much more problematic. A numerical procedure was developed using the least squares fitting algorithm 'lsqnonlin' that is incorporated in the MATLAB software package [29]. The values of R_1 and R_2 are determined by Eqs. (2), (3), (4), and (6) which are governed by the parameters C_{HH}, C_{FH}, τ_c and A. Good values of the correlation rate and the energy asymmetry are known from experiment, $\tau_c^{-1}(18\text{K}) = (9.8 \pm 0.1) \times 10^6 \text{s}^{-1}$ (Fig. 9) and $A/k_B = 80 \pm 3$K (Fig. 7). Therefore C_{HH} and C_{FH} were treated as fitting parameters in a non-linear fitting procedure to the data in Fig. 10 where Eqs. (2), (3), (4), and (6) were fitted to two sets of data, $R_1(B)$ and $R_2(B)$, simultaneously. The following best fit parameters were obtained;

$$C_{FH} = (1.1 \pm 0.2) \times 10^7 s^{-2};\ C_{HH} = (4.1 \pm 0.8) \times 10^8 s^{-2}$$

The best fits are shown as solid lines in Fig. 10 which show good correspondence with the data. Visual inspection identifies broad and narrow spectral density components; the former is evidently associated with the spectral density component $L(\omega_H - \omega_F)$ while the narrow component relates to a superposition of $L(\omega_H + \omega_F)$, $L(\omega_H)$ and $L(2\omega_H)$.

The temperature dependence of the bi-exponential spin–lattice relaxation rates R_1 and R_2 has been modelled using a reduced form of Eq. (7) for $\tau_c^{-1}(1/T)$ which omits the intermediate term involving a particular excited state. At 18 K the temperature is sufficiently low that the proton transfer rate is in the 'plateau' region and

the earlier measurement provides a good estimate of the ground state tunnelling rate, $k_0 \simeq \tau_c^{-1}(18\text{K}) = (9.8 \pm 0.1) \times 10^6 \text{s}^{-1}$. The value of the energy asymmetry $A/k_B = 80\text{K}$ is also known from experiment so that only values of τ_0^{-1} and ΔE_{act} are required in Eq. (7) to provide a model for the proton transfer rate as a function of temperature as the motion evolves between quantum and pseudo-classical regimes. Assuming the intermediate term in Eq. (7) is negligible ($\tau_{exc}^{-1} = 0$), $\tau_c^{-1}(1/T)$ has been modelled to provide $R_1(1/T)$ and $R_2(1/T)$ from Eqs. (2), (3), (4), and (6). The values of the Arrhenius rate parameters were chosen to be equal to the values determined for benzoic acid ($\tau_0^{-1} = 5 \times 10^{11}\text{s}^{-1}$, $\Delta E_{act} = 600\text{K}$ [7,11,26]) and the modelled behaviour is shown with solid lines in Fig. 7. No parameters have been adjusted in this analysis but the modelled behaviour represents the main features of the experimental data qualitatively well: the slope at low temperature, the position and depth of the high temperature minimum, the appearance of the low temperature shoulder, the ratio R_1/R_2 and the temperature above which the relaxation behaviour becomes mono-exponential. In detail there are some deviations between the modelled behaviour and experiment in the temperature region where the system is undergoing the transition from bi-exponential to mono-exponential behaviour. However, this is also the region where the intermediate term in the proton transfer rate, Eq. (7), would have greatest effect. Therefore, the models for heteronuclear spin–lattice relaxation and proton transfer dynamics provide generally good agreement with experimental observations.

6. Concluding remarks

For the earliest days of magnetic resonance, fixed-field NMR relaxation experiments have successfully been employed to investigate molecular dynamics. However, the interpretation of fixed-field data requires detailed theoretical models for the dynamics which is necessarily a source of systematic uncertainty, particularly where quantum mechanical effects are present. With the advent of field-cycling NMR it has become possible to directly map out the spectral density so that, for homonuclear systems at least, a (dynamical) model-free interpretation of the data provides accurate values of the correlation times and magnetic coupling constants. For heteronuclear spin systems, additional spectral density components are present. These are characterised by the same correlation times but appear with different widths when plotted as a function of B-field [23]. This introduces some complexity into the analysis of heteronuclear spin–lattice relaxation data but in this paper we have explored the variety of ways the multiple spectral density components can manifest themselves and some experimental protocols that can be used to resolve them. In so doing we have shown it is still possible to extract the molecular dynamical rates without imposing a theoretical model for the dynamics on the analysis so long as the B-field dimension is fully exploited.

In this investigation the two samples have been chosen to provide exemplars of a broad spectrum of heteronuclear relaxation behaviour. One important characteristic of a ^{19}F–^1H system is the similarity between the Larmor frequencies of the two spin species; the outcome is that the spectral density component $L(\omega_H - \omega_F)$ appears as much the broadest constituent in a plot of relaxation rate versus magnetic field. By contrast, the component $L(\omega_H + \omega_F)$ is much less conspicuous in saturation–recovery experiments since in practise it is indistinguishable from $L(2\omega_H)$.

In the case of 2,3-DFBA the relaxation was observed to be single exponential within experimental error and a satisfactory analysis was obtained by assuming the relaxation was dominated by the ^1H homonuclear contributions to ρ_l; this facilitated an effective determination of the molecular dynamics. However, it is undoubtedly the case that the ^{19}F–^1H interactions do contribute to the experimentally observed dipolar constant. In this example, which seems to be common to some other heteronuclear systems [13,23], the magnitude of σ is insufficient to incur observable bi-exponential relaxation behaviour. Nevertheless, the term in C_{FH} does makes a finite contribution to ρ_l but it is evident from Eq. (2) that since the dominant heteronuclear spectral density terms are $L(\omega_H)$ and $L(\omega_H + \omega_F) \approx L(2\omega_H)$ these cannot be separately identified from the homonuclear terms. Furthermore, in this limit the term $L(\omega_H - \omega_F)$ cannot be separately identified from the T_1^{-1} vs. B profile within experimental error. There is therefore, a small systematic uncertainty in the measured correlation rate values but given the dominance of the homonuclear terms and the similarity in the effective T_1^{-1} vs. B profiles, simulations show this is no more than the random statistical uncertainty in the measurements.

In the case where cross-relaxation is detectable our experiments on 2,3,5,6-TFBA have shown that plotting σ vs. B provides a very effective and accurate technique for determining the molecular correlation rates. Since the spectral density components are simply known in this case, and determined solely by heteronuclear terms, this technique seems to be superior to magnetisation–recovery measurements of the diagonal relaxation elements.

Acknowledgments

The construction of the field-cycling NMR spectrometer was funded by grants from the Royal Society (Paul Instrument Fund) and EPSRC.

References

[1] M.J. Knapp, K. Rickert, J.P. Klinman, Temperature dependent isotope effects in soybean lipoxygenase-1: correlating hydrogen tunnelling with protein dynamics, J. Am. Chem. Soc. 124 (2001) 3865–3874.
[2] N.S. Scrutton, Enzymes in the quantum world, Biochem. Soc. Trans. 27 (1999) 767–779.
[3] O. Klein, F. Aguilar-Parrilla, J.M. Lopez, N. Jagerovic, J. Elguero, H.H. Limbach, Dynamic NMR study of the mechanisms of double, triple and quadruple proton and deuteron transfer in cyclic hydrogen bonded solids of pyrazole derivatives, J. Am. Chem. Soc. 126 (2004) 11718–11732.
[4] J.M.L. del Amo, U. Langer, V. Torres, G. Buntkowsky, H.M. Vieth, M. Perez-Torralba, D. Sanz, R.M. Claramunt, J. Elguero, H.H. Limbach, NMR studies of ultrafast intramolecular proton tautomerism in crystalline and amorphous – *N,N′*-diphenyl-6-aminofulvene-1-aldimine: solid-state, kinetic isotope and tunnelling effects, J. Am. Chem. Soc. 130 (2008) 8620–8632.
[5] R. Kind, P.M. Cereghetti, C.A. Jeitziner, B. Zalar, J. Dolinišek, R. Blinc, Slater ice-rules and H-bond dynamics in KDP-type systems, Phys. Rev. Lett. 88 (2002) 195501.
[6] R. Blinc, J. Dolinišek, B. Zalar, Low temperature properties of proton and deuteron glasses, Z. Phys. B 104 (1997) 629–634.
[7] A.J. Horsewill, Quantum tunnelling in the hydrogen bond, Prog. Nucl. Magn. Reson. Spectrosc. 52 (2008) 170–196.
[8] E.R. Andrew, L. Latanowicz, Solid state proton transfer dynamics and the proton NMR 2nd moment and proton relaxation rates, J. Magn. Reson. 68 (1986) 232–239.
[9] A. Stöckli, B.H. Meier, R. Kreis, R. Meyer, R.R. Ernst, Hydrogen bond dynamics in isotopically substituted benzoic acid dimers, J. Chem. Phys. 93 (1990) 1502–1520.
[10] A. Heuer, U. Haeberlen, The dynamics of hydrogens in double well potentials – the transition of the jump rate from the low temperature quantum mechanical to the high temperature activated regime, J. Chem. Phys. 95 (1991) 4201–4212.
[11] D.F. Brougham, A.J. Horsewill, R.I. Jenkinson, Proton transfer dynamics in the hydrogen bonds: a direct measurement of the incoherent tunneling rate by NMR and the quantum-to-classical transition, Chem. Phys. Lett. 272 (1997) 69–74.
[12] W. Wu, D.L. Noble, A.J. Horsewill, The correspondence between quantum and classical mechanics: an experimental demonstration of the smooth transition between the two regimes, Chem. Phys. Lett. 402 (2005) 519–523.
[13] Q. Xue, A.J. Horsewill, M.R. Johnson, H.P. Trommsdorff, Isotope effects associated with tunneling and double proton transfer in the hydrogen bonds of benzoic acid, J. Chem. Phys. 120 (2004) 11107–11119.
[14] F. Noack, NMR field-cycling spectroscopy-principles and applications, Prog. Nucl. Magn. Reson. Spectrosc. 18 (1986) 171–276.

[15] R. Kimmich, E. Anoardo, Field-cycling NMR relaxometry, Prog. Nucl. Magn. Reson. Spectrosc. 44 (2004) 257–320.
[16] N. Bloembergen, E.M. Purcell, R.V. Pound, Relaxation effects in nuclear magnetic resonance absorption, Phys. Rev. 73 (1948) 679–712.
[17] J.L. Skinner, H.P. Trommsdorff, Proton transfer in benzoic acid crystals – a chemical spin boson problem – theoretical analysis of nuclear magnetic resonance, neutron scattering and optical experiments, J. Chem. Phys. 89 (1988) 897–907.
[18] L. Latanowicz, E.C. Reynhardt, Comment on 'The correspondence between quantum and classical mechanics: an experimental demonstration of the smooth transition between the two regimes' [Chem. Phys. Lett. 402 (2005) 519], Chem. Phys. Lett. 433 (2007) 444–449.
[19] A.J. Horsewill, Reply to the Comment on 'The correspondence between quantum and classical mechanics: an experimental demonstration of the smooth transition between the two regimes' [Chem. Phys. Lett. 402 (2005) 519], Chem. Phys. Lett. 433 (2007) 450–453.
[20] V.A. Benderskii, E.V. Vetoshkin, S.Yu. Grebenshchikov, L. von Laue, H.P. Trommsdorff, Tunneling splitting in vibrational spectra of non-rigid molecules. I. Perturbative instanton approach, Chem. Phys. 219 (1997) 119–142.
[21] A. Abragam, The Principles of Nuclear Magnetism, Clarendon Press, Oxford, 1961 (p. 294).
[22] A.J. Horsewill, W. Wu, Proton tunnelling in a hydrogen bond measured by cross-relaxation field-cycling NMR, J. Magn. Reson. 179 (2006) 169–172.
[23] W. Wu, D.L. Noble, J.R. Owers-Bradley, A.J. Horsewill, A ^{13}C field-cycling NMR relaxometry investigation of proton tunnelling in the hydrogen bond: dynamic isotope effects, the influence of heteronuclear interactions and coupled relaxation, J. Magn. Reson. 175 (2005) 210–221.
[24] A.J. Horsewill, A. Ikram, I.B.I. Tomsah, Hydrogen bond dynamics in tetrafluoroterephthalic acid studied by NMR and INS, Mol. Phys. 84 (1995) 1257–1272.
[25] A.J. Horsewill, I.B.I. Tomsah, Bi-exponential spin–lattice relaxation in solid hexfluoroactylacetone, Solid State Nucl. Magn. Reson. 2 (1993) 61–72.
[26] M.A. Neumann, D.F. Brougham, C.J. McGloin, M.R. Johnson, A.J. Horsewill, H.P. Trommsdorff, Proton tunnelling in benzoic acid crystals at intermediate temperatures: nuclear magnetic resonance and neutron scattering studies, J. Chem. Phys. 109 (1998) 7300–7311.
[27] D.L. Noble, I. Frantsuzov, A.J. Horsewill, Field-cycling NMR investigations of ^{13}C–^{1}H cross-relaxation and cross-polarisation: the nuclear solid effect and dynamics nuclear polarisation, Solid State Nucl. Magn. Reson. 34 (2008) 110–117.
[28] M. Plazanet, N. Fukushima, M.R. Johnson, A.J. Horsewill, H.P. Trommsdorff, The vibrational spectrum of crystalline benzoic acid: inelastic neutron scattering and density functional theory calculations, J. Chem. Phys. 115 (2001) 3241–3248.
[29] The MathWorks, Inc. Available from: <http://www.mathworks.com/products/matlab/>.